

Simulated Biosorption of Cd(II) and Cu(II) in Single and Binary Metal Systems by Water Hyacinth (*Eichhornia crassipes*) using Aspen Adsorption®

Allan N. Soriano ¹

Omar Nassif Orfiana ¹

Mark Brandon J. Pangon ¹

Aileen D. Nieva ¹

Adonis P. Adornado ^{*1}

¹ School of Chemical Engineering and Chemistry, Mapúa University, Manila

*e-mail: apadornado@mapua.edu.ph

Biosorption is becoming an attractive alternative for the removal of heavy metal from contaminated wastewaters since it offers low capital and operating costs. It has a great potential on heavy metal decontamination and the possibility of metal recovery. The study evaluated the performance of water hyacinth (*Eichhornia crassipes*) in a fixed bed column on sequestering heavy metals present in wastewaters. Column breakthrough curves at varying parameters were evaluated. The study used Aspen Adsorption® to simulate the biosorption process. Analysis of breakthrough curves for the single metal system shows that increasing both influent flow rate and initial metal concentration reduces the metal uptake of the column, while increasing bed height enhances the metal uptake of the column. Presence of both Cd(II) and Cu(II) in the system promotes competitive sorption processes. Analysis of the breakthrough curves for the binary metal system showed that copper ions adsorbed to the adsorbent are replaced by cadmium ions when the maximum capacity of the column is reached. This leads to the outlet concentration of Cu(II) exceeding its initial concentration. This phenomenon shows that Cd(II) has more affinity with *E. crassipes* than Cu(II).

Keywords: Aspen Adsorption®; biosorption; *Eichhornia crassipes*; heavy metal; water hyacinth

INTRODUCTION

One of the present day global concerns is wastewater management. Anthropogenic activities such as mining, smelting, electroplating, electro-osmosis, and coal-firing introduce wastewaters

containing metal contaminants to the environment (Papageorgiou et al., 2009). Heavy metals such as lead, cadmium, chromium, zinc, mercury, and copper are biologically toxic elements that can bioaccumulate, bioconcentrate, and biomagnify (Hu et al., 2007). As a result,

the removal of these toxins from industrial effluents has become an important priority that is reflected in a tightening enforcement of environmental regulations (Davis et al., 2003). Different methods such as chemical precipitation, electro dialysis, ion exchange, and reverse osmosis have been used in treating the metal contaminated wastewaters. However, these methods have been proven to be costly and energy intensive, making their implementation in large scale operations unviable. Adsorption, particularly biosorption, is becoming an attractive alternative for the removal of heavy metal from contaminated wastewaters (Dang et al., 2009).

Biosorption process represents an effective passive sequestration of organic and inorganic substance by certain types of non-living biomass (Diniz et al., 2008). The process involves liquid phase containing dissolved species (sorbate) and a solid phase (biosorbent) in which the sorbate is adsorbed due to the differences in the affinities of the sorbate specie to the different media, with the solid phase having higher affinity to the biosorbate (Gallarte, 2014). Biosorption offers many advantages such as low capital and operating costs, the selective removal of metals, the possibility of metal recovery, rapid kinetics of adsorption and desorption, and no sludge formation.

Recent studies on phytoremediation involved studying different plant species as potential biosorbent for industrial wastewater treatment. Among these, aquatic macrophytes have gained popularity due to its significant potential on heavy metal uptake from solutions

(Rubio et al., 1999; Maine et al., 2004; Mishra et al., 2009). Water hyacinth (*Eichhornia crassipes*) is a submerged aquatic plant commonly found in drainage channels and irrigation systems. Results from previous batch adsorption studies have determined the ability of the *E. crassipes* species, particularly its roots, to sequester metal ions from solutions (Liu et al., 2013; Mohanty et al., 2006; Módenes et al., 2011). Information from these batch studies, such as equilibrium and kinetic data, can be used in analyzing column dynamics in continuous adsorption processes.

Although there are numerous studies involving the use of aquatic macrophytes such as *E. crassipes* as biosorbent, most of these studies are done on laboratory scale batch experiments and often focused on the adsorption of only one heavy metal. This is rarely or never the case for actual wastewater coming from industrial facilities which contains a variety of heavy metal contaminants. The behavior of adsorption of some metals is affected by the presence of another metal species as different metals have different affinities with the binding sites during adsorption. Also, the presence of other metal ions affects the selectivity of the binding sites to the different ions present (Módenes et al., 2011; Saraswat and Rai, 2010; Mahamadi and Nharingo, 2010). In order for *E. crassipes* to be used as a biosorbent in an industrial scale fixed-bed column adsorption process, studying the information about the effects of different parameters on the column dynamics are essential.

The main objective of this study is to

simulate the continuous fixed-bed adsorption of Cd(II) and Cu(II) onto *E. crassipes* using Aspen Adsorption[®]. The specific objectives of this study includes determining the effects of varying different parameters such as initial metal concentration, bed height, and influent flow rate on the column dynamics by virtue of breakthrough curve analysis. Also, the effect of the presence of different metal species (binary metal system) on the column breakthrough curve will be discussed.

This study will be able to provide information on *E. crassipes* as biosorbent for metals Cu(II) and Cd(II) in both single and binary systems on a continuous fixed-bed adsorption process. The field of using process simulation in studying the effects of different parameters for an adsorption process will be explored. Also, the results of this study will be able to provide insight in designing an economically viable and eco-friendly alternative on removing heavy metals from wastewaters; or optimization of already existing heavy metal adsorption facilities.

METHODS

The biosorption of Cu(II) and Cd(II) by *Eichhornia crassipes* will be simulated using Aspen Adsorption[®] V8.4. The study is composed of three major sections: (1) the search for experimental data from previous studies involving *E. crassipes* as biosorbent with Cu(II) and Cd(II) as contaminants, (2) the simulation of the adsorption process on single and binary metal systems at varying column specifications, and (3) the treatment and

interpretation of results.

Experimental Data Sources

These are essential in obtaining the parameters required for the simulation. These parameters are data which Aspen Adsorption[®] is not able to provide. Moreover, experimental data can be used for validation of the data obtained from the simulation. Table 1 lists the parameters that are used along with the sources. The values for the maximum adsorption capacity of *E. crassipes* was obtained from the study of Módenes et al. (2011) where the stock solutions of Cd(II) and Cu(II) metals were prepared using their water-soluble salt forms CdCl₂ and CuCl₂. As per the study of Módenes et al. (2011), the adsorption of both Cd(II) and Cu(II) onto *E. crassipes* is best described by the Langmuir Isotherm which has the constant parameters presented in **Table 1**.

Simulation Parameters

As ion exchange is the principal mechanism of adsorption of heavy metals to water hyacinth (Saraswat and Rai, 2010; Zheng et al., 2009), ion exchange process will be used instead of liquid adsorption process. The process flow sheet diagram is constructed in the process flowsheet window which includes three blocks: (1) bed, (2) feed, and (3) product with streams S1 and S2 connecting the feed to the bed and the bed to the product respectively. The feed and product specifications, such as feed concentration and flow rates, can be managed in the feed block and product block respectively. The bed block is where the adsorbent and column parameters were provided for the simulation. **Figure 1**

Table 1. Experimental parameters used for the simulations.

Parameter	Value	Reference
q_{max} (IP1)		
Copper	0.615 meq·g ⁻¹	Módenes et al. (2011)
Cadmium	0.667 meq·g ⁻¹	Módenes et al. (2011)
b_L (IP2)		
Copper	0.444 L·meq ⁻¹	Módenes et al. (2011)
Cadmium	0.566 L·meq ⁻¹	Módenes et al. (2011)
Bulk density	0.031 g·cm ⁻³	Rani et al. (2014)
Particle density	0.023 g·cm ⁻³	Rani et al. (2014)
Pore space volume	2.2 ml·g ⁻¹	Rani et al. (2014)
Pore volume	13.75 cm ³ ·g ⁻¹	Rani et al. (2014)
Average Particle Diameter of <i>E. crassipes</i>	75 μm	Rani et al. (2014)

shows the process flowsheet used for all simulation runs in this study.

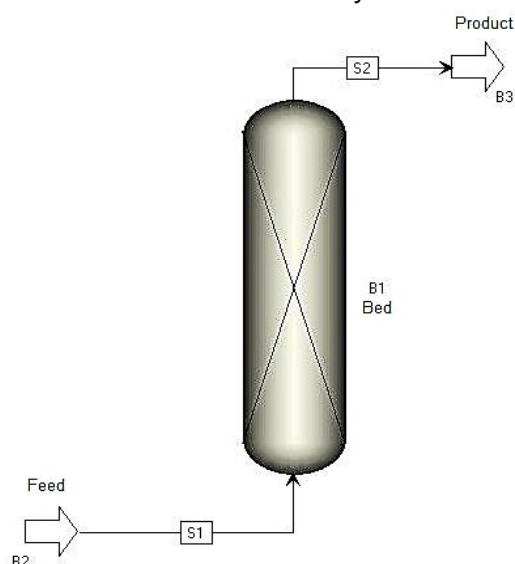


Fig. 1: Ion exchange process flowsheet in Aspen Adsorption®.

Physical and Chemical Properties of Metal Ions

The component list was configured prior to the set-up of the process flowsheet. The component list is configured using Aspen Properties®. The chloride salts of Cu(II) and Cd(II), which are CuCl₂ and CdCl₂, were used to match the study of Módenes et al. (2011). Aspen

Properties® provided the physical properties of these electrolytes in combination with water. ELECNRTL (Electrolyte Non-Random Two Liquid) is set as the property method, as it is the most versatile electrolyte property method in Aspen Adsorption®. It can handle any liquid electrolyte solution unless there is an association in the vapor phase. Also, ELECNRTL is fully consistent with the NRTL-RK (Non-Random Two Liquid-Redlich Kwong) property method for the molecular interactions are calculated exactly the same way, and therefore, can use the databank for binary molecular interaction parameters for the NRTL-RK property method. Aspen's Properties Electrolyte wizard was used to generate the electrolyte's chemistry. It was assumed that there was no salt and ice formation and that only water dissociation reactions were present. After the component list has been saved, it is converted to a component set in order to add another component, which is the counter ion. The addition of the counter ion component enables the observation of the behavior of

a theoretical counter ion during the adsorption process.

Feed and Product Specification Tables

In the feed and product blocks, specifications such as initial metal concentration, initial counter ion concentration, and flow rates can be specified. The ionic metals and theoretical counter ion were the only components on the list as water is a default component in Aspen Adsorption[®]. A theoretical counter ion component has been added to observe the behavior of a corresponding counter ion for a particular metal ion during the adsorption process. This gives us an insight on how fast the adsorbent is spent and how long can the adsorbent be used before it is needed to be regenerated.

The product concentration of the metal was initially set to zero in order to determine the breakthrough time for the column. Adapting the standards for effluents of the local setting, the breakthrough concentration for Cd(II) and Cu(II) was based on the DENR Administrative Order No. 35 (DAO 35). The effluent standard considered is for old and existing industries (OEI) for water class C, which is the classification of lakes, rivers, reservoirs used for industrial water supply. The breakthrough concentration (C_b) of Cd(II) and Cu(II) was set to $0.10 \text{ mg}\cdot\text{L}^{-1}$ and $0.50 \text{ mg}\cdot\text{L}^{-1}$ respectively.

The reversible model is chosen as the model type for the process. The density of the solvent, which in this case the density of water, is specified as $55.16 \text{ kmol}\cdot\text{m}^{-3}$. The initial and final concentration of both the metal ion and counter ion is given in

terms of equivalence per cubic meter ($\text{eq}\cdot\text{m}^{-3}$). The initial concentration of the heavy metal in the feed block is set to be equal to the final concentration of the counter ion on the product block and the initial concentration of the counter ion is set to be equal to the final concentration of the heavy metal in product block which is zero. By doing this, it is assumed that initially, all of the metal is able to be adsorbed by the adsorbent. The flow rate of the feed is also set in the feed block and is specified as a fixed value. This means that the flow rate is assumed to be all throughout.

Bed Specifications

The bed model assumptions for ion-exchange set by Aspen Adsorption[®] V8.4 are: (1) overall and component material balances apply for the liquid phase, (2) isothermal conditions apply, (3) plug flow or plug flow with axial dispersion applies, (4) the liquid stream pressure is constant (no frictional pressure drop), (5) the superficial velocity, thus, volumetric flow rate remain constant (The ion components are dilute so that the effect of adsorption on the overall mass balance is negligible.), (6) ideal mixing occurs in the aqueous phase (Since the ionic components are very dilute, overall molar volume remains constant), (7) changes in molar volume between distinct, sequentially fed fluids are allowed, (8) the total exchange capacity of the bed Q is constant, (9) a lumped mass-transfer rate applies with a liquid-film or solid-film resistance. This resistance is either linear, quadratic, or user-defined, (10) the mass-action equilibrium is one alternative model for

ion-exchange behavior. Others include the extended-Langmuir and extended Langmuir-Freundlich models. The set of equations that is used within the layer of the bed was configured using the tabs in the configure layer form. These tabs are the general tab, the material/momentum balance tab, the kinetic model tab, and the isotherm tab. Under the general tab, the discretization method and the number of nodes are specified. Considering the advantages and disadvantages, the chosen discretization method is the Upwind Differencing Scheme 1 (UDS 1) as it is the one of the best standard discretization method in terms of accuracy, stability and simulation time. The UDS 1 is a first-order upwind differencing scheme based on a first-order Taylor expansion. The first-order (convection) term is:

$$\frac{\partial \Gamma_i}{\partial z} = \frac{\Gamma_i - \Gamma_{i-1}}{\Delta z} \quad (1)$$

While the second-order (dispersion) term is approximated with a second order differencing scheme:

$$\frac{\partial^2 \Gamma_i}{\partial z^2} = \frac{\Gamma_{i+1} - 2\Gamma_i + \Gamma_{i-1}}{\Delta z^2} \quad (2)$$

The number of nodes was set to a default at 20 nodes. The overall material balance used by Aspen Adsorption® to simulate ion-exchange processes is expressed as:

$$v_l \frac{\partial p_l}{\partial z} + \varepsilon_i \frac{\partial p_l}{\partial t} = 0 \quad (3)$$

Where v_l is the liquid velocity, p_l is the liquid molar density, z is the axial coordinate, ε_i is the interparticle voidage,

and t is for time. This equation accounts for the fact that, during an ion-exchange cycle, solvents of different densities are being used in different production, purge and regeneration stages. Density remains unchanged as a result of the ion-exchange process itself.

Each ionic species in the liquid phase, fed into the ion-exchange column, is governed by the following material balance equation:

$$-\varepsilon_i E_z \frac{\partial^2 c_k}{\partial z^2} + v_l \frac{\partial c_k}{\partial z} + \varepsilon_i \frac{\partial c_k}{\partial t} + J_k = 0 \quad (4)$$

Where E_z is the axial dispersion coefficient, c_k is the ion concentration in liquid phase, and J_k is the ion material transfer rate.

The mass transfer rate J_k between the bulk liquid and the resin is given by:

$$J_k = (1 - \varepsilon_i) \frac{\partial w_k}{\partial t} \quad (5)$$

Where the uptake rate $\partial w_k / \partial t$ can, be determined by a solid film linear driving force relationship, such as:

$$\frac{\partial w_k}{\partial t} = MTC_{sk} (w_k^* - w_k) \quad (6)$$

Where MTC_{sk} is the solid mass transfer coefficient, w_k^* is the ion loading in equilibrium with liquid phase concentration (eq·m³), and w_k is the ion loading on adsorbent (eq·m³).

The number of counter ions being released from the resin and entering the liquid phase is determined from the number of ions exchanged from the liquid

phase - the total charge of both liquid and resin must remain neutral:

$$J_b = \sum_{\substack{k=1 \\ k \rightarrow b}}^{nc} J_k \quad (7)$$

Where J_b is the counter ion material transfer rate. Hence, the behavior of the exchanged counter ion in the liquid phase can be described by:

$$-\varepsilon_i E_z \frac{\partial^2 c_b}{\partial z^2} + v_l \frac{\partial c_b}{\partial z} + \varepsilon_i \frac{\partial c_b}{\partial t} + \sum_{\substack{k=1 \\ k \rightarrow b}}^{nc} J_k = 0 \quad (8)$$

Where c_b is the counter ion concentration in liquid phase.

In the material/momentum balance tab, the basic assumptions about material dispersion in the liquid phase for ion exchange processes are specified. There are several assumptions that can be chosen on the material balance assumption box which are: convection only, convection with constant dispersion, convection with estimated dispersion, and convection with user-defined dispersion. In this study, convection with estimated dispersion is chosen. With this, the dispersion coefficient varies along the length of the bed and is estimated using the correlation developed by Slater in 1991:

$$\frac{v_i d_p}{E_z} = 0.2 + 0.011 \left(\frac{Re}{\varepsilon_i} \right)^{0.48} \quad (9)$$

Where, E_z is the axial dispersion coefficient, v_i is the liquid velocity, ε_i is the interparticle voidage, d_p is the particle diameter, and Re is the Reynolds number

which can be calculated using the equation below.

$$Re = \frac{\rho_l M_l d_p v_l}{\mu} \quad (10)$$

Where μ is the liquid viscosity, ρ_l is the liquid molar density, and M_l is the liquid molecular weight.

The overall mass transfer of ionic components between the bulk liquid phase and the adsorbed phase must overcome two resistances: (1) mass transfer resistance located in the boundary layer surrounding the particle and (2) mass transfer resistance inside the resin particle, with the later determining the overall mass transfer rate. Aspen Adsorption® lumps the overall resistance to mass transfer into a single overall factor. The type of mass transfer resistance are selected from: (1) the film model assumption, (2) the kinetic model assumption, (3) the form of lumped resistance, and (4) the form of mass transfer coefficient; which are found under the kinetic model tab.

For the film model assumption, the solid film was chosen as it expresses the mass transfer driving force as a function of the solid phase concentration. For the kinetic model assumption, the lumped resistance in linear function was used. Here, the mass transfer driving force for component k is expressed as a function of the solid phase concentration. The equation for this assumption is the same equation as used in Eqn. (6).

The mass transfer coefficient was set to be constant. Thus, the mass transfer coefficient for each component will be the same throughout the bed. The value for

the mass transfer coefficient was supplied in the specification table of the bed layer. Lastly, under the isotherm tab, the Langmuir Isotherm was chosen.

Calculation of some missing parameters were done to satisfy the bed specification table. This includes the inter-particle voidage (ε_i), intra-particle voidage (ε_p), total resin capacity (Q), and the mass transfer coefficient (MTC) of the metal ions. The inter-particle and intra-particle voidage of the bed were calculated using Eqns. (11) and (12), respectively.

$$\text{Pore space volume} \times \text{Bulk density} = \text{Inter-particle voidage} \quad (11)$$

$$\text{Pore volume} \times \text{Bulk density} = \text{Intra-particle voidage} \quad (12)$$

Eqn. (11) yielded a value of $0.06800 \text{ m}^3 \cdot \text{m}^{-3}$ for the inter-particle voidage and Eqn. (12) yielded a value of $0.31625 \text{ m}^3 \cdot \text{m}^{-3}$ for the intra-particle voidage. Also, IP1 is converted from $\text{meq} \cdot \text{g}^{-1}$ to $\text{mg} \cdot \text{g}^{-1}$ which yielded a value of 19.54 for Cu(II) and 37.49 for Cd(II).

For the binary metal solution, the total resin capacity was assumed to be the summation of the maximum capacities of the adsorbent for each metal. The capacity ($\text{eq} \cdot \text{m}^{-3}$) can be computed by the following equation:

$$N_o = \rho q_o (1 - \varepsilon_i) \quad (13)$$

Where ρ is the density of the medium at $23,000 \text{ g} \cdot \text{m}^{-3}$, q_o is the maximum capacity of the metal ($\text{eq} \cdot \text{g}^{-1}$), and ε_i is the intra-particle voidage which is equal to $0.31625 \text{ m}^3 \cdot \text{m}^{-3}$. The resulting capacities were $10.4894 \text{ eq} \cdot \text{m}^{-3}$ and $9.6716 \text{ eq} \cdot \text{m}^{-3}$ for Cd

and Cu respectively. Thus, the total resin capacity for the binary metal system would be $20.1610 \text{ eq} \cdot \text{m}^{-3}$.

The external mass transfer coefficient of particles in a fixed-bed column can be estimated using the equation as follows:

$$Sh = 2 + 1.1 Re^{0.6} Sc^{\frac{1}{3}} \quad (14)$$

Where $Sh = k_c D_p / D_{AB}$, $Re = D_p u \rho / \mu$, and $Sc = \mu / \rho D_{AB}$ (Perry and Green, 2008). Substituting the definitions of Re , Sc , and Sh in Eqn. (14) yields:

$$\frac{k_c D_p}{D_{AB}} = 2 + 1.1 \left(\frac{D_p u \rho}{\mu} \right)^{0.6} \left(\frac{\mu}{\rho D_{AB}} \right)^{\frac{1}{3}} \quad (15)$$

Where D_p is the particle diameter, D_{AB} is the mass diffusivity of solute, u is the fluid velocity, ρ is the density of the solution, and μ is the viscosity of the solution. It is assumed that the solution is very dilute and that the metal ions will have no effect on the density and viscosity of the solution, and thus, the density and viscosity of water at 30°C were used. Water has a density of $995.650 \text{ kg} \cdot \text{m}^{-3}$ and viscosity of $7.9720 \times 10^{-4} \text{ kg} \cdot \text{m} \cdot \text{s}^{-1}$ at 30°C .

D_{AB} is defined as the mass diffusivity of solute A in solvent B. However, in aqueous solutions, electrolytes dissociates in cations and anions, hence the average mass diffusivity of the electrolyte is a combination of the individual diffusion coefficients of both the cation and anion. Using Eqn. (16), the over-all mass diffusivity of the electrolytes CdCl_2 and CuCl_2 in water were computed as follows

$$D_{AB} = \frac{n_+ + n_-}{\frac{n_+}{D_+} + \frac{n_-}{D_-}} \quad (16)$$

Where, n_+ is the valence of the cation, n_- is the valence of the anion, and D_i is the diffusion coefficient of individual ion (Geankoplis, 2005). The diffusion coefficients of the ions resulting from the dissociation of the aforementioned electrolytes are $D_{Ca(II)} = 7.920 \times 10^{-10} \text{ m}^2 \cdot \text{s}^{-1}$, $D_{Cu(II)} = 7.140 \times 10^{-10} \text{ m}^2 \cdot \text{s}^{-1}$, and $D_{Cl^-} = 2.13 \times 10^{-10} \text{ m}^2 \cdot \text{s}^{-1}$ (Gallarte, 2014). The resulting mass diffusivity (D_{AB}) were $2.816 \times 10^{-10} \text{ m}^2 \cdot \text{s}^{-1}$ for Cd(II) and $2.780 \times 10^{-10} \text{ m}^2 \cdot \text{s}^{-1}$ for Cu(II).

As the mass transfer coefficient is a function of fluid velocity, the mass transfer coefficient will also change when the flow rate is varied. Thus, the mass transfer coefficient was calculated for each flow rate used. **Table 2** shows the list of flow rates used together with the corresponding mass transfer coefficient.

In the process flowsheet window, the breakthrough flowsheet form was added. This form graphs the breakthrough curve for the process and was configured to display the outlet concentration of both the metal ion and the counter ion on the product block. Opening the breakthrough form will show the breakthrough plot window with the concentrations of the metal ion and counter ion on the y-axis and time at the x-axis.

Table 2. Mass transfer coefficients at different flow rates.

Flow Rate, L/s	Mass Transfer Coefficient (k_c), m/s	
	Cd(II)	Cu(II)
0.05	0.00038	0.00038
0.10	0.00057	0.00057
0.25	0.00098	0.00098
0.50	0.00148	0.00148
0.75	0.00189	0.00189
1.00	0.00224	0.00224

Simulation

There were three process scenarios that were approached in the single metal system which were varying bed height, varying flow rate, and varying initial metal concentration; while in the binary metal system, varying ratio of the initial metal concentration was tackled. The simulation is started by initializing the process and then proceeding to dynamic mode of the simulation. In the dynamic mode, the plot of the breakthrough curve is produced as time progresses. The change in the concentration of the metal ion and counter ion was observed in real time. This was seen in the breakthrough plot window.

To study the effects of bed height on the breakthrough time and the breakthrough curve of the column, the bed height (m) was set on three different values: 0.50, 0.75, and 1.00. The simulations to determine the effects of bed height were run while holding the initial metal concentration and flow rate constant.

To study the effects of the feed flow rate on the breakthrough time and breakthrough curve of the column, the flow rate ($\text{L} \cdot \text{s}^{-1}$) was set on six different values: 0.05, 0.10, 0.25, 0.50, 0.75, and 1.00. The simulations to determine the effects of flow rate were run while holding the initial metal concentration and bed height constant.

To study the effects of the initial metal concentration on the breakthrough time and breakthrough curve of the column, the initial metal concentration (ppm) was set on six different values: 2, 5, 10, 15, 25, and 50. However, Aspen Adsorption®

required the value of the initial metal concentration to be expressed in $\text{eq}\cdot\text{m}^{-3}$. Thus, the concentrations were converted in terms of $\text{eq}\cdot\text{m}^{-3}$. **Table 3** shows the values of the initial metal concentration in $\text{eq}\cdot\text{m}^{-3}$.

Table 3. Concentrations of heavy metals in $\text{eq}\cdot\text{m}^{-3}$.

Concentration, ppm	Cadmium	Copper
2	0.0356	0.0629
5	0.0889	0.1574
10	0.1779	0.3147
15	0.2669	0.4721
25	0.4448	0.7868
50	0.8896	1.5737

As for the binary metal system study, the total initial concentration for the Cd-Cu metal system was set at 25 ppm with varying percentage of cadmium and copper. **Table 4** shows the concentrations used for this binary system in $\text{eq}\cdot\text{m}^{-3}$. The flow rate and bed height were held constant at $0.10 \text{ L}\cdot\text{s}^{-1}$ and 1.00 m respectively.

Table 4. Concentrations of Cd(II) and Cu(II) at varying percentage of 25 ppm in $\text{eq}\cdot\text{m}^{-3}$.

Percent	Cadmium	Copper
25%	0.1112	0.1967
50%	0.2224	0.3934
75%	0.3336	0.5901

The concentration combinations used were 25% Cd-75% Cu, 50% Cd-50% Cu, and 75% Cd-25% Cu.

RESULTS AND DISCUSSION

Biosorption of Cd(II) and Cu(II) onto Water Hyacinth (*E. crassipes*)

The study used water hyacinth roots as its biosorbent to sequester Cd(II) and Cu(II). The biosorption of Cd(II) and Cu(II) with cations (counterion) is attributed to ion exchange, and complex formation with functional groups on the surface of the roots (Saraswat and Rai, 2010; Mohanty et al., 2006; Liu et al., 2013; Zheng et al., 2009). As per the limitations of the study, ion exchange process was considered as the main mechanism of adsorption. In an ion exchange process, as presented in **Figure 2**, the counterion (Ca^{2+}) that is bounded onto the functional groups (R^-) present on the surface of the biosorbent such as carboxyl, amine, hydroxyl, sulfhydryl, imidazole, phosphate, and sulphate, will be displaced by the metal ion (Cd^{2+}) since the ions in the fluid phase have a greater affinity for the bound groups than those originally present. Generally, the biosorbent has a fixed total charge capacity, so one ionic solute is exchanged for another while maintaining charge neutrality. The counterions

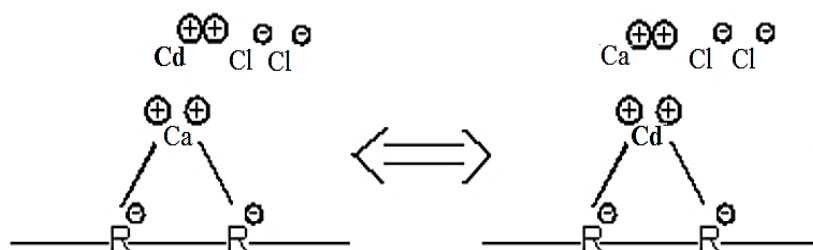


Fig. 2: Ion exchange of Cd(II) with calcium counterion.

bounded onto the functional groups present in water hyacinth roots are Ca^{2+} , K^+ , Mg^{2+} , and Na^+ (Akinwande et al., 2013). Among these, Ca^{2+} was the counterion as it has the same charge as Cu(II) and Cd(II) (Zheng et al., 2009) and Cd(II) (Murithi et al., 2014). Ca^{2+} is also present in high amounts based on the report of Akinwande et al., (2012) (see **Table 5**) which strongly suggests that it is a suitable counterion for Cd(II) and Cu(II) .

Table 5. Mineral composition of water hyacinth.

Macro mineral	g/100g DM
Calcium	3.08
Phosphorus	0.28
Magnesium	0.65
Potassium	4.13
Sodium	0.13

The saturation of the biosorbent can be related through the hydrated ionic radius of the cations present. The hydrated ionic radius of the Ca^{2+} (counterion) in the biosorbent is 0.112 nm, while for Cd(II) and Cu(II) ions, the hydrated ionic radius are 0.096 nm and 0.156 nm, respectively (Persson, 2010). Based on the presented hydrated radii of the cations, the Cu(II) hydrated radius is larger than the counterion while the Cd(II) hydrated radius is smaller than the counterion. This means that there are more available sites for adsorption for Cd(II) since its hydrated ionic radius is smaller compared to Cu(II) . Also, larger hydrated ionic radius of the metal ions leads to a quicker saturation of the adsorption sites, caused by steric hindrance (Chiban et al., 2008). Based on the results, it can be seen that the breakthrough time for Cu(II) is shorter

than Cd(II) , this can be attributed to the Cu(II) ions having large hydrated ionic radius. Although Cu(II) ions provide stronger attraction due to its higher electronegativity as compared to Cd(II) ion ($1.9 > 1.69$), Cd(II) exchange with counterions is still more favored due to steric hindrance.

Effect of Initial Metal Concentration

The effects of initial metal ion concentration were determined by varying the initial metal ion concentration from 2 ppm to 50 ppm. The increase in initial metal concentration led to a shorter breakthrough time and in turn also led to reduced volume treated by the column before it is saturated. **Figures 3 and 4** showed the breakthrough curves for a column set at a bed height of 1.00 m and a flow rate of 0.50 L/s with varying initial metal (Cd and Cu , respectively) concentration from 2 ppm to 50 ppm while **Table 6** presented the breakthrough time and breakthrough volume. The breakthrough curves were determined by plotting the dimensionless concentration (effluent concentration, C , divided by initial metal concentration, C_0) against time.

The driving force necessary to overcome all mass transfer resistances of the metal ions between the aqueous and solid phases is provided by the initial metal concentration (Mahamadi and Zambara, 2013). Looking at the equation used by Aspen Adsorption[®] in calculating the rate of metal uptake of the column (Eqn. 6), the rate of metal uptake by the adsorbent is directly proportional to the mass transfer coefficient and the

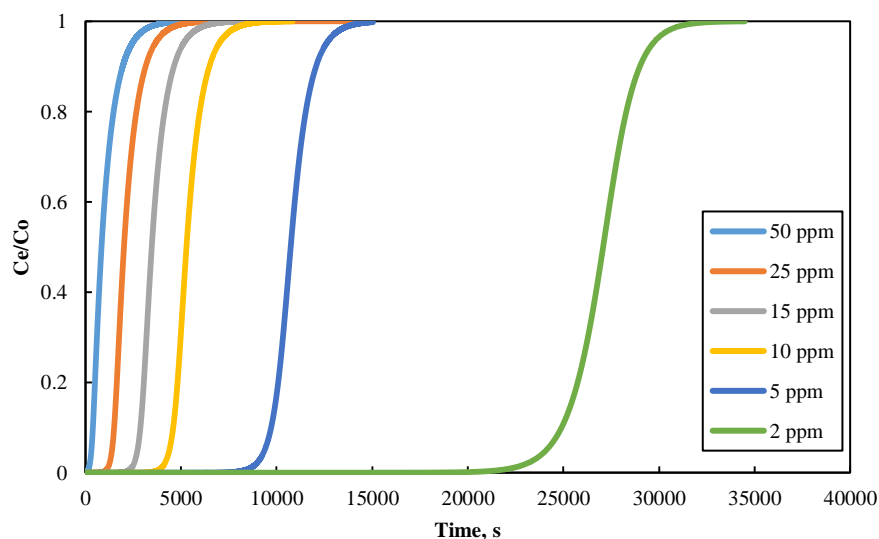


Fig. 3: Breakthrough curve for varying initial concentration of Cd at bed height of 1.00 m and flow rate of 0.50 L/s.

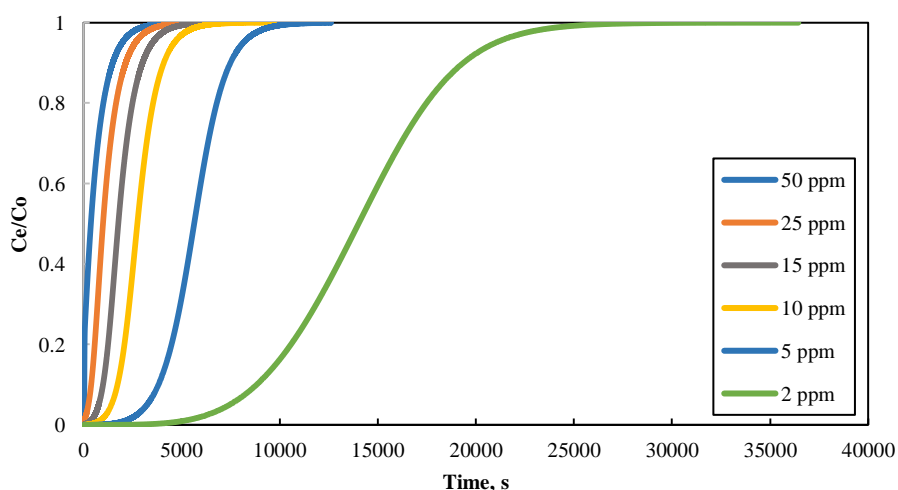


Fig. 4: Breakthrough curve for varying initial concentration of Cu at bed height of 1.00 m and flow rate of 0.50 L/s.

difference between the concentration of the metal on the adsorbent and the concentration of the metal in equilibrium with the liquid phase.

Hence, as the initial metal concentration is increased, the concentration gradient increases as well and so as the rate of metal uptake by the adsorbent. The faster adsorption rate caused by a high initial concentration

results in a shorter breakthrough time as the adsorbent reaches its adsorption capacity sooner. This can be observed from the results of the simulation, wherein the breakthrough time decreases from 24,105 s to 61 s for Cd(II) and 11,250 s to 29 s for Cu(II) as the initial metal concentration is increased from 2 ppm to 50 ppm. It is also observed that at high initial concentration, the breakthrough

Table 6. Breakthrough time and breakthrough volume of cadmium and copper at constant bed height of 1.00 m and flow rate of 0.50 L/s.

Initial concentration, ppm	Cadmium		Copper	
	Breakthrough time, s	Breakthrough volume, L	Breakthrough time, s	Breakthrough volume, L
50	61	30.5	29	14.5
25	1,034	517.0	100	50.0
15	2,320	1,160.0	658	329.0
10	3,954	1,977.0	1,422	711.0
5	8,932	4,466.0	2,114	1,910.0
2	24,105	12,052.5	11,250	5,625.0

curves are steeper at shorter breakthrough time. On the other hand, at lower initial concentration, the breakthrough curves lose its steepness and achieve a longer breakthrough time.

Similar observations were reported in the sorption of Cr(VI) onto *E. crassipes* stem (Singha et al., 2012) and adsorption of Cu(II) onto *E. crassipes* immobilized by alginate (Mahamadi and Zambara, 2013) wherein the authors attributed the decrease in breakthrough time to the increased concentration gradient providing greater driving force for the sorption of the metals leading to the faster saturation of the column. Furthermore, it is observed that as the initial metal concentration is increased, the breakthrough curves become steeper. The steepness of a breakthrough curve generally describes the extent to which the capacity of an adsorbent bed is utilized. A steeper breakthrough curve indicates that more of the bed is used efficiently for the adsorption process (Geankoplis, 2005).

Effect of Bed Height

Figures 5 and 6 illustrated the breakthrough curves obtained for the adsorption Cu(II) and Cd(II) ions on varying bed heights (m) of 0.50, 0.75, and 1.00 at a constant flow rate of 0.10 L·s⁻¹ and initial concentration of 15 ppm. The breakthrough times observed for Cd(II) were 5,700 s, 8,544 s, and 14,104 s for 0.50 m, 0.75 m, and 1.00 m bed height, respectively. The results show that the breakthrough time increases as the bed height is increased, which is also observed in other runs at different concentrations and flow rates. This can be attributed to the increased contact time, increased available surface area, or a combination of both that provides better sorption of the metal ions (Mahamadi and Zambara, 2013).

The amount of adsorbent in the bed can be estimated by assuming the column as a cylinder with constant diameter. The mass of the adsorbent in the column can be obtained by the equation:

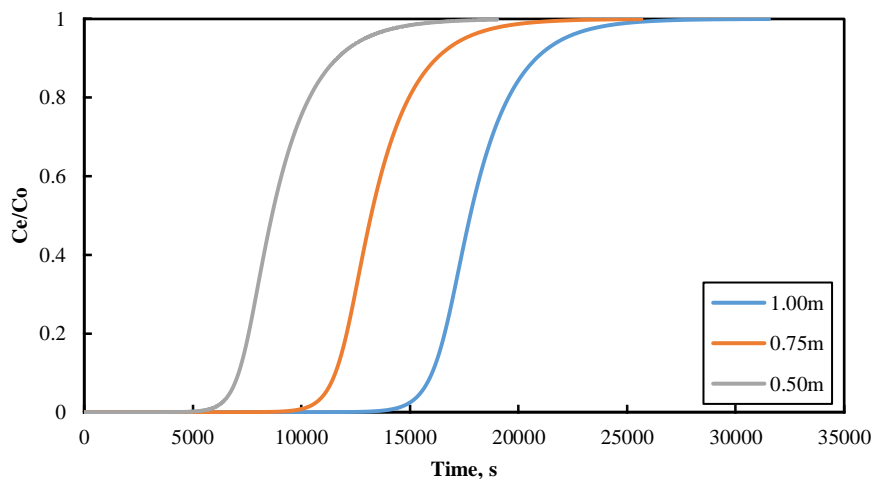


Fig. 5: Cd (II) breakthrough curves at varying bed height at constant flow rate of $0.10 \text{ L}\cdot\text{s}^{-1}$ and initial concentration of 15 ppm.

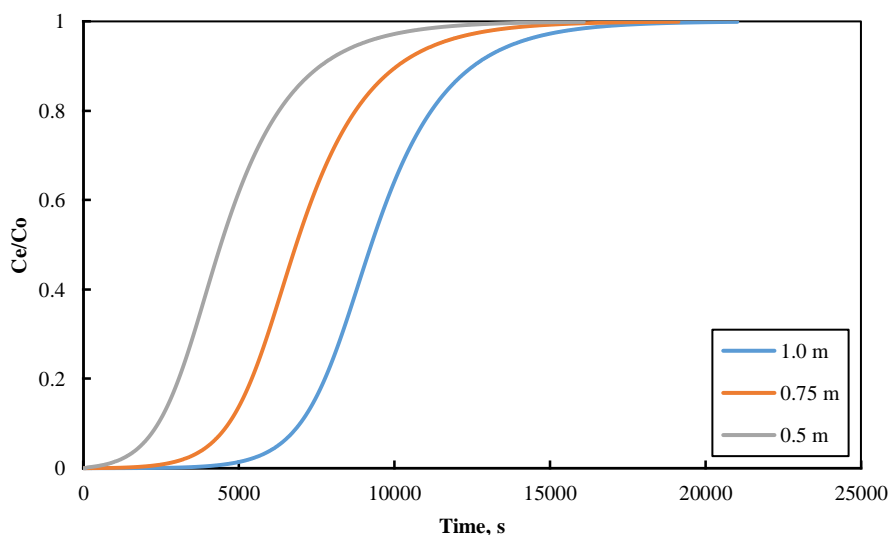


Fig. 6: Cu(II) breakthrough curves at varying bed height at constant flow rate of $0.10 \text{ L}\cdot\text{s}^{-1}$ and initial concentration of 15 ppm.

$$m_b = \frac{1}{4} \pi D^2 H_b \rho_b \quad (17)$$

Where D is the column diameter, H_b is the bed height, and ρ_b is the bulk density of the adsorbent. As seen in Eqn. (17), as the bed height is increased, the available surface area, thus, amount of available sites for adsorption also increases as there is more adsorbent available. A similar

observation was also reported in a study of the adsorption of Methylene blue by cellulose nanocrystal-alginate hydrogel beads (Mohammed et al., 2016). The authors attributed the longer breakthrough time and larger breakthrough volume to the increased number of available sites for adsorption when the bed height is increased. A lower

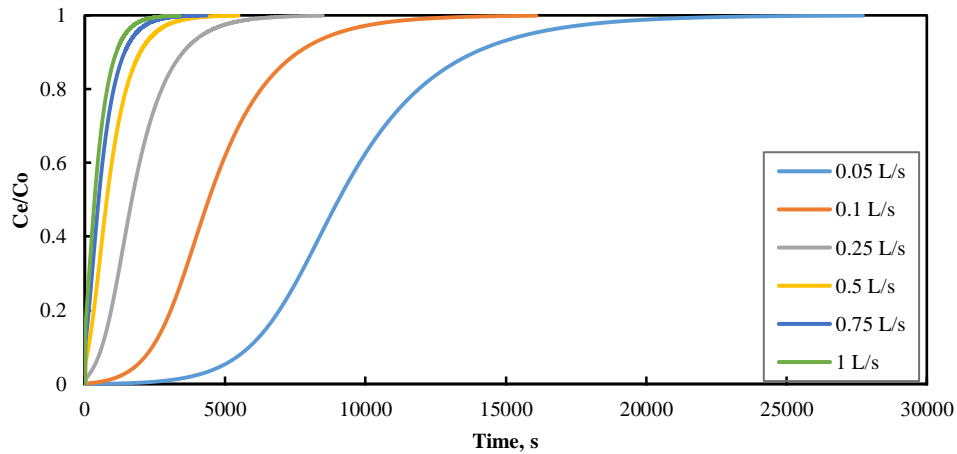


Fig. 7: Cd(II) breakthrough curves at varying flow rates at constant bed height of 0.50 m and initial concentration of 15 ppm.

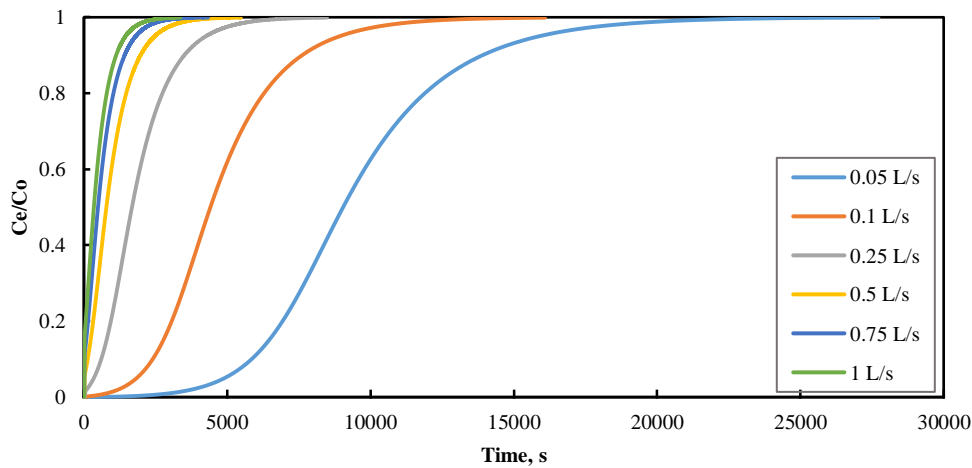


Fig. 8: Cu(II) breakthrough curves at varying bed height at constant flow rate of 0.10 L·s⁻¹ and initial concentration of 15 ppm.

bed height implies a smaller capacity of the bed to adsorb metal ions from the solution, thus, leading to a faster breakthrough and exhaustion time. Also, in lower bed heights, axial dispersion is considered as the predominant mass transfer phenomenon which reduces the diffusion of metal ions (Singha et al., 2012).

Effect of Flow Rates

The effect of influent or feed flow rate

was studied by varying the flow rates at a constant bed height and initial metal concentration. The breakthrough curves were determined by plotting effluent concentration against time. **Figures 7 and 8** illustrated the breakthrough curves obtained for the adsorption Cu(II) and Cd(II) ions on varying flow rates (L·s⁻¹) of 0.05, 0.10, 0.25, 0.50, 0.75 and 1.00 at a constant bed height of 0.50 m and initial concentration of 15 ppm. **Table 7** presented the breakthrough time and

breakthrough volume.

As seen in Figures 7 and 8, at higher flow rate, the front of the adsorption zone quickly reached the top of the column and that the column was saturated early. The observed breakthrough time for cadmium decreased from 10,830 s to 22 s and 4,384 s to 9 s for copper. These results show that an increase in flow rate decreases the breakthrough time, which is also observed in all performed simulations. Also, higher influent flow rate resulted to the column being exhausted earlier. The decrease in both breakthrough time and exhaustion time resulted in steeper breakthrough curves as shown in Figures 7 and 8, and reduces the volume treated efficiently by the column until reaches breakthrough point, as shown in Table 7. The reduction in metal uptake is attributed to insufficient residence time of the metal ions in the column and the diffusion limitations of the solute into the pores of the sorbent at higher flow rates (Simate and Ndlovu, 2015). In other words, if the residence time of the solute in the column is not long enough for adsorption equilibrium to be reached at the given flow rate, the metal

solution leaves the column before the equilibrium occurs, thus gave rise to a shorter time for saturation (Simate and Ndlovu, 2015).

Similar findings were found by Mahamadi and Zambara (2013) where copper is adsorbed using water hyacinth fixed on alginate. This study shows that at higher influent flow rate, the uptake of copper ions onto the biosorbent is reduced due to the decrease in contact time between the copper ions and the biosorbent, thus resulting in the solute leaving the column before equilibration occurs. Similar results were found by Babu and Gupta (2005) where they simulated a fixed bed adsorption column that also resulted in the decrease of metal uptake at higher influent flow rates.

As the solution flows through the bed column, axial dispersion or mixing may occur. If mixing occurs, the efficiency of the bed in removing the metal ions is reduced. To check whether axial dispersion is significant or not, Eqn. (18) was used.

$$Pe = ReSc = \left(\frac{dv\rho}{\mu}\right)\left(\frac{\mu}{\rho D}\right) = \frac{dv}{D} \quad (18)$$

Table 7. Breakthrough time and breakthrough volume for varying influent flow rate of cadmium and copper at constant bed height of 0.50 m and initial concentration of 15 ppm.

Influent flow rate, L·s ⁻¹	Cadmium		Copper	
	Breakthrough time, s	Breakthrough volume, L	Breakthrough time, s	Breakthrough volume, L
1.00	22	22.0	9	9.0
0.75	108	81.0	13	9.8
0.50	335	167.5	22	11.0
0.25	1,238	309.5	220	55.0
0.10	4,575	457.5	1,542	154.2
0.05	10,830	541.5	4,384	219.2

Where d is bed diameter, v is the volumetric flow rate, ρ is the liquid density, μ is liquid viscosity, and D is diffusivity. The bed diameter, liquid density, liquid viscosity, and diffusivity are constant while volumetric flow rate varies. Peclet number (Pe) quantifies the degree of dispersion introduced into the system. If Pe is less than 30, axial dispersion is significant; if it is greater than 100, the bed operates under near plug flow conditions; and if it is towards positive infinity, the bed operates under plug flow condition. The calculation of Pe in all considered flow rates in the

study lead to same results, the values are toward positive infinity. This concludes that axial dispersion is not significant in the system due to the bed is operating under plug flow condition.

Effect of Other Metal Species

Three simulations were done on the binary system at varying fractions of Cu(II) and Cd(II). The total concentration was set at 50 ppm with fractions of 25% Cd-75% Cu, 50% Cd-50% Cu, and 75% Cd-25% Cu. The simulation results are presented in **Figure 9** and **Table 8**.

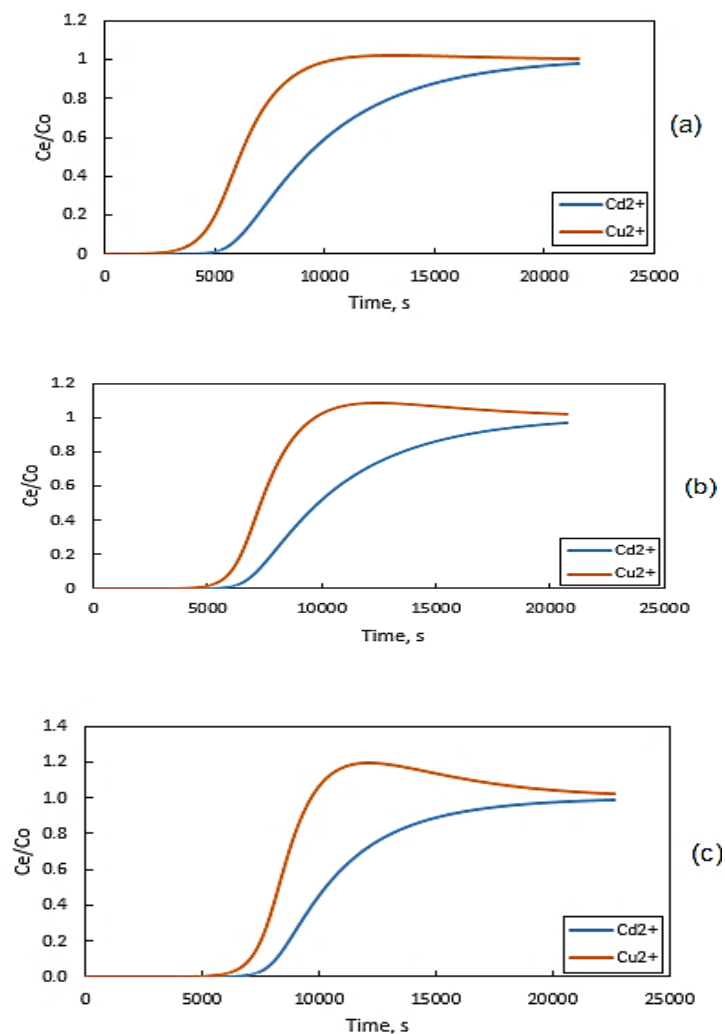


Fig. 9: Binary system breakthrough curves at 50 ppm: (a) 75% Cd-25% Cu; (b) 50% Cd-50% Cu; (c) 25% Cd-75% Cu.

Table 8. Breakthrough time for Cd(II) and Cu(II) in binary metal system.

Composition	Breakthrough Time, s	
	Cadmium	Copper
25% Cd - 75% Cu	4,833	1,503
50% Cd - 50% Cu	5,556	3,870
75% Cd - 25% Cu	6,396	5,127

The shape of the breakthrough curves for the binary metal system shows a different shape than those observed for the single component system simulated as shown in Figure 9. The most noticeable difference is that Cd(II) behaves similarly as observed in single component system, while Cu(II) exceeds or overshoots its initial concentration indicated by the ratio C/C_0 being greater than 1. The origin of the overshoot may be attributed to the nature of the sorption itself. When the maximum capacity of the column is reached, species with lower affinity with the adsorbent are replaced by other species with higher affinity and displacement of the previously sorbed species occurs (Escudero et al., 2013). This phenomenon typically indicates competitive sorption processes. Initially, both Cd(II) and Cu(II) are adsorbed by the adsorbent. However, as the course progress, Cd(II) ions displaces the Cu(II) ions previously adsorbed. The liberation of the Cu(II) ions results to the outlet concentration of Cu(II) exceeding its initial concentration.

It is also observed in the breakthrough curves that the overshoot of Cu(II) increases as the percentage of Cd(II) increases. This can again be attributed to the greater affinity of Cd(II) with *E.*

crassipes. As the adsorbent favors the adsorption of Cd(II), it tends to accommodate more of the Cd(II) ions than the Cu(II) ions. Hence, increasing the concentration of Cd(II) increases the number of Cd(II) ions available to displace the Cu(II) ions that were previously adsorbed thereby increasing the amount of Cu(II) released.

From Table 8, it can be seen that the breakthrough time for Cd(II) is longer than Cu(II) in all of the experiments. This indicates that Cd(II) has better affinity with *E. crassipes* and is able to be adsorbed longer than Cu(II) before it reaches its breakthrough concentration and saturate the column. Also, it can be observed that the breakthrough time for Cu(II) increases as its initial concentration is decreased. This can be attributed to the affinity of Cu(II) to the adsorbent as well. Since Cu(II) has a weaker affinity with *E. crassipes* compared to Cd(II), less of it is adsorbed. Hence, at high concentrations of Cu(II), the adsorbent is easily saturated with it and reaches its breakthrough concentration much faster than at a lower concentration.

The affinity of the metals with the biosorbent may be related with the Langmuir constant b in which a higher value of b indicates better affinity of the adsorbent to the adsorbate. The value of

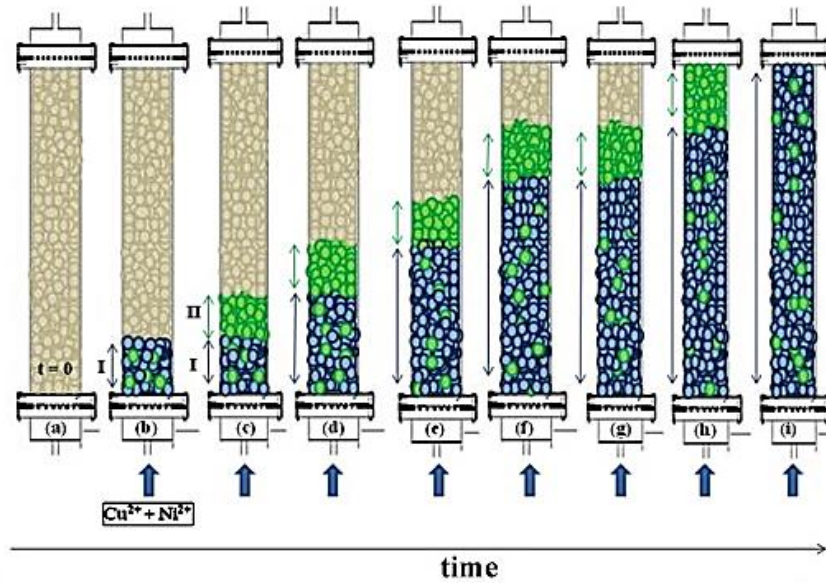


Fig. 10: Development of a binary mixture during an adsorption process in a column (Adapted from Kleinubing et al. 2012).

the Langmuir constant for Cu(II) is lower compared to Cd(II) (see Table 1). Hence, Cd(II) has better affinity with *E. crassipes* than Cu(II) and will be adsorbed more by the biosorbent. The same pattern was observed in the study of Escudero et al. (2013) for the adsorption of Cu(II), Cd(II), Ni(II), and Pb(II) onto grape stalks waste. From the equilibrium studies, the reported affinity order was $Pb > Cu > Cd > Ni$ based on the Langmuir isotherm parameters. It was observed in the column studies that Cu(II) overshoots in binary mixtures of Pb(II) while Ni(II) and Cd(II) overshoots by over 60% in the presence of Cu(II) and Pb(II) in binary mixtures. It was reported that Pb(II) does not overshoot in any of the binary mixture case with Cu(II), Cd(II), and Ni(II) which follows their initial findings between affinity of the metals. Similar observations were reported by Kleinubing et al. (2012) for the adsorption of Cu(II) and Ni(II) by *Sargassum filipendula*. The authors attributed the overshoot of Ni(II) ions to

the greater affinity of Cu(II) with the adsorbent.

Kleinubing et al. (2012) explained the development of a binary mixture during the adsorption process in a column using a schematic diagram shown in **Figure 10**.

In Figure 10, the initial stage of the process is represented by step (a) wherein no solution is flowing into the column. In step (b), the binary solution begins flow inside the column and metal ions are adsorbed into the biosorbent near the entrance of the column. The blue shade represents the metal species that has better affinity with the biosorbent while the green shade represent the metal species with weaker affinity. The metal species with better affinity with the biosorbent will be preferentially retained in the lower region of the bed (steps (b) to (i)); this makes the leading solution flowing through the column to be relatively concentrated with the metal specie having weaker affinity with the biosorbent (green

shade), which is practically sorbed under single component condition without competition. At some point, region I becomes saturated and the binary solution will begin to flow to region II in which the initially sorbed metal with weaker affinity is replaced by the metal species with better affinity with the biosorbent. The sequence (step (c) to (h)) continues until it reaches the saturation of the column and the release of the metal with weaker affinity to the outlet solution causes the concentration of the metal with weaker affinity to exceed its initial concentration, hence, the overshoot in the breakthrough curve.

CONCLUSION

The effect flow rate, initial metal concentration, and bed height on the performance of *E. crassipes* on sequestration of Cd(II) and Cu(II) in a fixed bed column were investigated through breakthrough curve analysis. The said parameters proved to have significant effects on the performance of the adsorption column. Analysis of breakthrough curves shows that high initial metal concentration results to having shorter breakthrough time and steeper shape of the breakthrough curve. This can be attributed to the higher concentration gradient providing a stronger driving force necessary to overcome all mass transfer resistances of the metal ions between the aqueous and solid, which increases the adsorption rate through the bed. However, a shorter breakthrough time indicates inefficient

adsorption and that there is a lesser metal uptake. Therefore, having a lower initial metal concentration is more favorable over a higher initial metal concentration.

Increasing the influent flow rate results to a shorter breakthrough time and steeper breakthrough curve. The reduction in metal uptake by the increase in flow rate is mainly attributed to the insufficient contact time between the metal ions and the biosorbent. At high flow rates, the solute leaves the column before equilibrium is achieved and results to a faster rise in the outlet concentration which ultimately leads to a shorter breakthrough. Therefore, a lower influent flow rate is desired for better adsorption.

Increasing the bed height resulted to a longer breakthrough time. This is attributed to the amount of adsorbent present in the column. As bed height is increased, the amount of available adsorbent is also increased, hence, available sites for adsorption increases as well. This allows more metal ions to be accommodated, thus, leads to a longer time for the metals to reach its breakthrough concentration. A lower bed height implies a smaller capacity of the bed to adsorb metal ions from the solution, thus, leading to a faster breakthrough and exhaustion time. Also, in lower bed heights, axial dispersion is considered as the predominant mass transfer phenomenon which reduces the diffusion of metal ions onto the adsorbent layer.

Presence of both Cd(II) and Cu(II) in the binary system promotes competitive sorption processes. Analysis of the breakthrough curves for the binary system

showed that Cu(II) ions, tends to exceed its initial concentration. This was described as Cu(II) previously adsorbed to the adsorbent were being replaced by Cd(II) ions as the maximum capacity of the column is reached. The release of Cu(II) ions resulted to the outlet concentration of Cu(II) exceeding its initial concentration. Therefore, it can be concluded that, compared to Cu(II), Cd(II) has better affinity with *E. crassipes* and will be adsorbed better by the biosorbent.

REFERENCES

1. Akinwande, V. O., A. A. Mako and O. J. Babayemii (2013). Biomass yield, chemical composition and the feed potential of water hyacinth (*Eichhornia crassipes*, Mart.Solms-Laubach) in Nigeria. *Int. J. of AgriScience*, **3**, 659-666.
 2. Chiban, M., H. Benhima, F. Sinan, P. Seta, and M. Persin (2008). Removal of lead and cadmium ions from aqueous solution by adsorption onto micro-particles of dry plants. *Colloids Surf. B: Biointerfaces*, **61**, 10-16.
 3. Dang, V. B. H., H. D. Doan, T. Dang-Vu and A. Lohi (2009). Equilibrium and kinetics of biosorption of cadmium (II) and copper (II) ions by wheat straw. *Bioresour. Technol.*, **100**, 211-219.
 4. Davis, T. A., B. Volesky and A. Mucci (2003). A review of biochemistry of heavy metal biosorption by brown algae. *Water Res.*, **37**, 4311-4330.
 5. Diniz, V., M. E. Weber, B. Volesky and G. Naja (2008). Column biosorption of lanthanum and europium by *Sargassum*. *Water Res.*, **42**, 363-371.
 6. Escudero, C., J. Poch and I. Villaescusa (2013). Modelling of breakthrough curves of single and binary mixtures of Cu(II), Cd(II), Ni(II), and Pb(II) sorption onto grape stalks waste. *Chem. Eng. J.*, **217**, 129-138.
 7. Gallarte, B. (2014). Cd(II), Cu(II), and Pb(II) Simulated Adsorption by *Sargassum cristaefolium*: Affinity, Competitiveness, and Selectivity. MS Thesis. School of Chemical Engineering and Chemistry, Mapúa Institute of Technology, Philippines.
 8. Geankoplis, C. J. (2005). Principles of Transport Processes and Separation Processes, Pearson Education South Asia PTE. LTD., Philippines.
 9. Babu, B. V. and S. Gupta (2005). Modeling and simulation of fixed bed adsorption column: effect of velocity variation. *i-Manager's JFET*, **1**, 60.
 10. Hu, Z., X. Yang, A. Gao and X. Wei (2007). Remediation of mycorrhiza on Cd contaminated soil. *J. China Univ. of Mining and Tech.*, **36**, 237.
 11. Kleinubing, S. J., E. Guibal, E. A. da Silva and M. G. C. da Silva (2012). Copper and nickel competitive biosorption simulation from single and binary systems by *Sargassum filipendula*. *Chem. Eng. J.*, **184**, 16-22.
 12. Liu, Z., X. Li, Z. Na, D. Lu and S. Liu (2013). Adsorption, concentration and
-

- recovery of aqueous heavy metal ions with the root powder of *Eichhornia crassipes*. *Eco. Eng.*, **60**, 160-166.
13. Mahamadi, C. and P. Zambara (2013). High Cu removal from water using water hyacinth fixed on *alginate*. *Environ. Chem. Lett.*, **11**, 377-383.
14. Mahamadi, C. and T. Nharingo (2010). Competitive adsorption of Pb^{2+} , Cd^{2+} and Zn^{2+} ions onto *Eichhornia crassipes* in binary and ternary systems. *Bioresour. Technol.*, **101**, 859-864.
15. Maine, M. A., N. Suñé and S. C. Lager (2004). Chromium bioaccumulation: comparison of the capacity of two floating aquatic macrophytes. *Water Res.*, **38**, 1494-1501.
16. Mishra, V. K., B. D. Tripathi and H. K. Kim (2009). Removal and accumulation of mercury by aquatic macrophytes from an open cast coal mine effluent. *J. Hazard. Mater.*, **172**, 749-754.
17. Módenes, A. N., F. R. Espinoza-Quinones, D. E. G. Trigueros, F. L. Lavarda, A. Colombo and N. D. Mora (2011). Kinetic and equilibrium adsorption of Cu (II) and Cd (II) ions on *Eichhornia crassipes* in single and binary systems. *Chem. Eng. J.*, **168**, 44-51.
18. Mohammed, N., N. Grishkewich, H. A. Waeijen, R. M. Berry and K. Tam (2016). Continuous flow adsorption of methylene blue by cellulose crystal-alginate hydrogel beds in fixed bed columns. *Carbohydr. Polym.*, **136**, 1194-1202.
19. Mohanty, K., M. Jha, B. C. Meikap and M. N. Biswas (2006). Biosorption of Cr (IV) from aqueous solutions by *Eichhornia crassipes*. *Chem. Eng. J.*, **117**, 71-77.
20. Murithi, G., C. O. Onindo, E. W. Wambu and G. K. Muthakia (2014). Removal of cadmium (II) ions from water by adsorption using water hyacinth biomass. *BioResources*, **9**, 3613-3631.
21. Papageorgiou, S. K., F. K. Katsaros, E. P. Kouvelos and N. K. Kanellopoulos (2009). Prediction of binary adsorption isotherms of Cu^{2+} , Cd^{2+} and Pb^{2+} on calcium alginate beads from single adsorption data. *J. Hazard. Mater.*, **162**, 1347-1354.
22. Perry, R. H. and D. W. Green (2008). Perry's Chemical Engineering Handbook, 8th Edition, McGrawHill Professional Publ., New York.
23. Persson, I. (2010). Hydrated metal ions in aqueous solution: How regular are their structures? *Pure Appl. Chem.*, **82**, 1901-1917.
24. Rani, J. M., M. Murugan, P. Subramaniam and E. Subramanian (2014). A study on water hyacinth *Eichhornia crassipes* as oil sorbent. *J. Appl. Nat. Sci.*, **1**, 134-138.
25. Rubio, J., R. W. Smith and I. A. H. Schneider (1999). Effect of mining chemicals on biosorption of Cu^{2+} by the non-living biomass of the macrophyte *Potamogeton lucens*. *Miner. Eng.*, **12**, 255-260.
26. Saraswat, S. and J. P. N. Rai (2010). Heavy metal adsorption from aqueous solution using *Eichhornia crassipes* dead biomass. *Int. J. Miner. Process.*, **94**, 203-206.
27. Simate, G. S. and S. Ndlovu (2015). The removal of heavy metals in a packed bed column using immobilized cassava peel waste biomass. *J. Ind. Eng. Chem.*,
-

- 21**, 635-643.
28. Singha, S., U. Sarkar, S. Mondal and S. Saha (2012). Transient behavior of packed column of *Eichhornia crassipes* stem for the removal of hexavalent chromium. *Desalination*, **279**, 48-58.
29. Zheng, J. C., H. M. Feng, M. H. W. Lam, P. K. S. Lam, Y. W. Ding and H. Q. Yu (2009). Removal of Cu(II) in aqueous media by biosorption using water hyacinth roots as a biosorbent material. *J. Hazard. Mater.*, **171**, 780-785.
-